Journal of Magnetic Resonance 307 (2019) 106583

Contents lists available at ScienceDirect

Journal of Magnetic Resonance

journal homepage: www.elsevier.com/locate/jmr

X-nuclei hyperpolarization for studying molecular dynamics by DNP-FFC

Bulat Gizatullin, Carlos Mattea, Siegfried Stapf*

FG Technische Physik II/Polymerphysik, Technische Universität Ilmenau, D-98684 Ilmenau, Germany

ARTICLE INFO

Article history:
Received 17 July 2019
Revised 20 August 2019
Accepted 21 August 2019
Available online 23 August 2019

Keywords:
NMR
DNP
FFC
X-nuclei
Overhauser effect
Hyperpolarization
TEMPO

ABSTRACT

Dynamic Nuclear Polarization methods are used for improving the quality of the NMR data, opening new possibilities by increasing both the sensitivity and the selectivity in NMR relaxation experiments. Recently, Fast Field Cycling relaxometry combined with DNP was introduced, demonstrating that molecular dynamics studies in the presence of natural or artificial radicals are indeed feasible under conditions where the signal-to-noise ratio is frequently critical. In this work, the extension of NMR relaxation dispersion beyond ^{1}H NMR, by hyperpolarization of X-nuclei, is demonstrated. Overhauser effect via nitroxide radicals in simple (low viscous) liquids and saline solutions was observed for ^{2}H, ^{7}Li and ^{13}C nuclei at ambient temperature. Substantial NMR signal enhancement up to several hundred was achieved for the studied samples. An advanced approach for reconstructing of the original relaxation dispersion of pure substances is used to eliminate the effect of the additional radical relaxivity of the X-nuclei.

1. Introduction

Dynamic Nuclear Polarization (DNP) Fast Field-Cycling (FFC) is a new combination of methods that was recently reported [1] to provide a signal-enhanced access to the frequency dependence of the longitudinal relaxation time, or relaxation dispersion (NMRD), for studying molecular dynamics in various systems [2–5]. The main concept of FFC [6] is using electronic switching between different magnetic field strengths in the range of typically 0.1 mT–1 T within a few milliseconds, which allows one to obtain information about molecular motions in the corresponding time scale of 10^{-8}–10^{-3} s in a variety of samples of fundamental interest, including proteins [7], liquid crystals [8,9], crude oil [10,11], and polymer systems [12]. Furthermore, cross relaxation [13,14] and electron-nuclear interaction features [15] can be investigated using the FFC technique. However, low sensitivity due to the limitation of the polarization field leaves many materials out of reach of the FFC method, such as diluted solutions, or X-nuclei systems with target nuclei with low natural abundance or low gyromagnetic ratio γ and, correspondingly, low thermal polarization. One of the main approaches to increasing sensitivity in NMR measurements is hyperpolarization. A variety of different hyperpolarization techniques are now available that allow to generate an NMR signal enhancement of up to several thousand for applications in spectroscopy and MRI studies. However, approaches such as changing the phase state as in dissolution DNP [16], designing chemical reactions in CIDNP [17,18] or the necessity to use gas as a hyperpolarization agent in SABRE [19,20], are frequently not applicable for molecular dynamics studies in viscous liquids, polymer melts and solutions. Thus, DNP is suggested as a suitable technique to obtain hyperpolarization in the above-mentioned systems.

DNP as a method assumes using radicals as a source of unpaired electron spins from which polarization is "borrowed". The use of the microwave field to manipulate electron energy levels saturation makes it possible to transfer higher polarization from the electron spin system to the nuclear spin system, while both are coupled to each other. The higher polarization of the electrons due to the higher gyromagnetic ratio compared to the nuclei theoretically allows to achieve corresponding NMR signal enhancements of several thousands in the case of ^{13}C, ^{2}H and ^{7}Li nuclei. Despite hardware limitations and undesirable sources of DNP enhancement reduction, such as quadrupolar relaxation and competition between scalar and dipolar electron-nucleus interactions, relatively high values of DNP enhancement in X-nuclei system were reported [15,21–24]. The implementation of DNP to the FFC methods requires the use of additional hardware such as a double resonance probe [25,26], a microwave bridge and the corresponding pulse protocols [27].

The Overhauser DNP effect (OE) which often dominates in liquids and solutions generates maximum enhancement when electron levels are saturated and the microwave irradiation frequency equals the Larmor electron frequency. Of course, this requires the existence of a corresponding electron nuclear coupling

* Corresponding author.
E-mail address: Siegfried.Stapf@tu-ilmenau.de (S. Stapf).

https://doi.org/10.1016/j.jmr.2019.106583
1090-7807/

and interaction which is modulated by processes such as translational or rotational diffusion with a rate being high enough to provide a significant contribution to the spectral density component at the electron Larmor frequency. This is commonly observed for liquids at low or intermediate magnetic field strength. However, it has also been shown theoretically and experimentally that OE remains effective even at high fields above 10 T [28], where it is preferably related with fast sub-ps local dynamics. Enhancements on the order of the theoretical limit, i.e. of up to several hundredfold, were already achieved for the abundant nuclei ^{1}H and ^{19}F in a variety of systems such as polymer melts [2] and solutions [29], oils [3] and simple liquids [30]. A preliminary study [1] of ^{13}C relaxation showed the potential of DNP FFC for studying the dynamics in systems by means of X-nuclei relaxation.

The requirement of having stable radicals present in the samples as a source of unpaired electrons, usually in the form of a low concentration of organic radicals such as TEMPO [31,32] or BDPA [33], necessarily leads to additional contributions to the total NMR relaxation rate [34,35]. If a significant signal enhancement is desired, the corresponding radical concentrations often leads to a relaxation rate contribution that is similar or larger than the intrinsic nuclear relaxation rate, and furthermore possesses its individual frequency dependence which masks the actual NMRD behavior of the sample that is required for verifying models for molecular dynamics. However, under the assumption that the radical-driven relaxivity is proportional to the radical concentration in homogeneous systems, the true nuclear relaxation dispersion can be recovered by using a difference approach [36] where results obtained at two or more radical concentrations are compared to each other. The main area of interest for the implementation of the difference approach is in systems with a low thermal polarization, which renders reliable relaxation times measurements within reasonable experimental time unfeasible. X-nuclei systems are one of the focus areas due to the low natural abundance of some isotopes, such as ^{13}C, and the relatively low gyromagnetic ratio of nuclei, such as ^{2}H, ^{7}Li etc. Despite the existence of a small number of studies of NMRD of X-nuclei systems, such as deuterated polymer systems [37], and D_2O in hydrated proteins [38] and in porous media [39], a considerable paucity of NMR studies of NMRD on X-nuclei is observed in the literature.

One of the advantages of using deuterated samples in molecular dynamics studies is the prevailing quadrupolar relaxation, which is almost entirely related to intramolecular dynamics, allowing one to neglect the intermolecular interactions contribution to the relaxation [39–41]. On the other hand, low thermal polarization and low sensitivity, consequently, requires time consuming experiments even for fully deuterated substances.

Lithium ions remain of considerable interest in the field of battery research; while published field-cycling studies of ^{7}Li [42] have demonstrated the feasibility of exploiting thermal polarization with dedicated hardware, the low γ certainly suggests that lithium studies will benefit from signal enhancement, particularly if the ions exist at low concentration. ^{7}Li DNP-FFC is thus considered in this paper as a feasibility study being representative for a number of low-γ ionic species such as ^{23}Na or ^{39}K.

The ^{13}C isotope is of paramount importance in metabolic and MRI studies, and is thus frequently studied in high-field DNP investigations [15,43–45]. However, the low natural abundance in combination with the low gyromagnetic ratio of ^{13}C nuclei puts even further constraints on the feasibility of extended studies. Furthermore, scalar contribution to the electron-nuclear interaction, which effects on ^{13}C DNP enhancement, is a matter of detailed investigations [15,43,46]. In this work, we are employing ^{13}C-enriched species for demonstrating the feasibility of DNP-FFC also for this nucleus, and comment on the potential of related applications in the future.

In this contribution, applications of DNP-FFC and the difference approach to improve quality of the NMRD data of X-nuclei systems, such as a deuterated liquid (benzene-d_6) in porous silica and an aqueous solution of LiCl, is presented. Additionally, the potential applications of using DNP-FFC to obtain relaxation properties of ^{13}C containing species are discussed on the example of benzene-d_6 with a natural abundance of ^{13}C. Standard dynamics models are used to fit DNP and NMRD data.

2. Methods

Samples of radical solutions were prepared using deuterated benzene-d_6 (99.5%, Deutero GmbH, Germany). An aqueous solution of 6 M LiCl (>99%, Carl Roth GmbH, Germany) was prepared with bidistilled deionized water. In order to generate the DNP effect, 2,2,6,6-Tetramethylpiperidine 1-oxyl (TEMPO) (98%, Sigma-Aldrich) and 4-Hydroxy-2,2,6,6-tetramethylpiperidine 1-oxyl (TEMPOL) (97%, Sigma-Aldrich) were used as radicals in the benzene-d_6 and LiCl aqueous solution, respectively. The radicals were dissolved in the respective liquids to obtain concentrations of 100 and 200 mM of TEMPO in benzene-d_6 and between 3.5 and 89 mM of TEMPOL in LiCl aqueous solution. The radical solutions as well as the bulk liquids were filled into 2.5 mm inner diameter (3 mm outer diameter) borosilicate glass tubes (Wilmad-LabGlass, U.S.A.), which were flame-sealed immediately. All samples were stored at +5 °C and were measured within 1 week of preparation.

Monodisperse silica fine particles were purchased from Sigma Aldrich. The grade A380 is characterized by an average particle diameter of 7 nm and a specific surface of 380 ± 30 m^2/g. The silica particles in 3 mm tubes were saturated by 100 and 200 mM TEMPO solutions in benzene-d_6, resulting in an amount of solution of 1.5 g per g of silica after centrifugation at 5000 rpm during 15 min and removing excess solution on the top of the sample.

The benzene sample for ^{13}C DNP was prepared by dissolving TEMPO in $^{13}C_6D_6$ (99% of ^{13}C and 99% of ^{2}H, Sigma-Aldrich) to obtain 70, 135 and 320 mM solutions, respectively. The sample with 70 mM of TEMPO was degassed by two freeze-thawing cycles under continuous pumping (30 mbar) and were subsequently flame-sealed.

The radical concentrations in the samples were controlled by employing a benchtop EPR spectrometer Magnettech 5000 (Magnettech, Freiberg Instruments, Freiberg, Germany).

DNP experiments and relaxation dispersion measurements were performed using a FFC relaxometer (Spinmaster FFC2000, Stelar, Mede, Italy) and a home-built DNP console with the probes combining an RF coil for excitation and detection of the NMR signal and a microwave resonator operating at X-band (~9.5 GHz microwave frequency) in the TM_{110} mode with a conversion factor c = 16 $\mu T/W^{-0.5}$, and at S-band (~2 GHz) with an Alderman-Grant resonator with c = 80 $\mu T/W^{-0.5}$ [25,26], respectively. For the purpose of measuring DNP spectra and standard NMRD measurements on the FFC relaxometer, an advanced pulse sequence including microwave irradiation during the polarization interval and a CPMG pulse sequence during signal acquisition was used [1,47]. The measurements of pure benzene-d_6 and LiCl water solution were performed using 10 mm tubes and a standard NMR 10 mm probe for conventional NMRD measurements.

For detection, the probes were tuned to 3.2 MHz (^{2}H and ^{13}C) and 4.4 MHz (for ^{7}Li), respectively, with the detection field set at the corresponding strength of 0.49 T, 0.30 T and 0.27 T. Signal acquisition was realized with a CPMG pulse sequence. All signal decays were fitted to a monoexponential function. All experiments were carried out at room temperature (293 K).

The temperature was controlled by heated dry air flow. The heating in DNP experiments at 5 W microwave power did not exceed 3–5 degrees. Pre-adjustment of temperature and dummy scans [25] were used to achieve a constant temperature of the sample during all experiments. Due to the impossibility of direct measurement of sample temperature the latter was controlled by comparison of the measured relaxation times under microwave irradiation and previously obtained temperature dependence of corresponding relaxation times without microwave irradiation during the polarization time interval. To eliminate microwave heating effects of the resonator itself during the polarization time, preliminary tests of different recycle delay times at particular microwave power and experimental parameters were performed. The optimal microwave power for performing NMRD experiments was estimated from power dependencies of enhancement for particular samples as the point when a further increase of the microwave power leads to an increase of the enhancement by a factor less than the corresponding time penalty which is necessary to dissipate additional power from resonator heating due to the microwave irradiation [25]. In the current setup, the necessary time to dissipate the adsorbed power after using 1 W of microwave irradiation during 1 s was 4 s at 20 l/min of cooling airflow. The obtained values of microwave power for the studied system were estimated in the range of 2.5–4.3 W.

3. Theory and models

3.1. DNP

At steady state DNP conditions, the DNP enhancement by OE is given by [48,49]:

$$E = \frac{P_{DNP}}{P_{TP}} = 1 - \xi f s \left|\frac{\gamma_e}{\gamma_n}\right|, \tag{1}$$

where γ_e and γ_n are the gyromagnetic ratios of the electron and nuclear spins, respectively, and P_{DNP} and P_{TP} are the polarizations of the nuclear spins in the hyperpolarized and the thermal state. The three parameters ξ, f and s in the right-hand side of Eq. (1) are the coupling, leakage and saturation factors, respectively, which are defined as:

$$\xi = \frac{w_2 - w_0}{w_0 + 2w_1 + w_2} = \frac{w_2 - w_0}{R_{1para}}, \tag{2}$$

$$f = \frac{R_{1para}}{R_1}, \tag{3}$$

where

$$R_1 = R_{1para} + R_{10} = r_{1rad}c + R_{10} \tag{4}$$

and w_1, w_2 and w_0 are the relaxation rates for single-, double- and zero-quantum transitions due to coupling with an electron spin. R_{10} is the nuclear spin-lattice relaxation rate measured in the absence of the radicals, whereas r_{1rad} is the radical-induced relaxivity normalized to concentration c. For a single, homogeneous EPR line, the saturation factor is given by [50]:

$$s = \frac{\gamma_e^2 B_1^2 T_{1e} T_{2e}}{1 + \gamma_e^2 B_1^2 T_{1e} T_{2e}}, \tag{5}$$

where B_1 is the magnetic field strength of the microwave field, and T_{1e} and T_{2e} are the corresponding electron relaxation times.

The coupling factor describes the efficiency of electron-nucleus cross relaxation processes to the paramagnetic relaxivity. The leakage factor f constitutes the paramagnetic relaxation contribution to the nuclear relaxation rate, while the saturation factor s describes the efficiency of the microwave irradiation.

In the ideal case, when saturation of electron levels and concentration of radicals are sufficiently high to generate conditions of s and f approaching 1, the coupling factor ξ plays the role of the restricting factor of DNP enhancement via OE, exhibiting, according to (1), the maximal enhancement levels of, e.g. -4270ξ for ^{2}H nuclei. A positive enhancement is attributed to the prevailing of scalar interaction with the maximal value of $\xi = -1$, while the dipolar coupling limit approaches the value of $\xi = 0.5$ with a corresponding negative net enhancement, i.e. an antiphase signal compared to the thermal polarization NMR signal. However, in real systems both contributions may exist, thus reducing the experimentally observed DNP enhancement [51].

The saturation factor s can be separated into two factors $s = s_{rel}(P)s_{max}(c)$ which depend on the microwave power and radical concentration, respectively, and where $s_{max}(c)$ depends on the number of electron spin transitions and on exchange effects mixing them, with $1/3 < s_{max} < 1$ for ^{14}N nitroxide radicals. By using Eq. (5) the relative saturation factor is written as [30]:

$$s_{rel}(P) = \frac{P/P_{half}}{1 + P/P_{half}}, \tag{6}$$

where $P_{half} = \left(\gamma_e^2 C^2 T_{1,e} T_{2,e}\right)^{-1}$ is a fitting parameter for which $s_{rel}(P_{half}) = 0.5$, while $\gamma_e B_1 = \gamma_e C\sqrt{P}$ depending on the strength of the microwave field in the resonator with conversion factor C.

From the power dependency of the enhancement $E(P)$, the limiting value extrapolated to infinite power enhancement E_{max} can be calculated by [30]:

$$E(P) = 1 - (1 - E_{max})\frac{P/P_{half}}{1 + P/P_{half}}, \tag{7}$$

The maximum of the DNP saturation factor for a system with three EPR transitions, as is the case for the ^{14}N nitroxide radical with its triplet hyperfine splitting due to the I = 1 nuclear spin, is then given by [30,52]:

$$s_{max}(c) = \frac{1}{3}\left[3 - 4\left(2 + \frac{k_{exch}c}{W_e}\right)^{-1}\right], \tag{8}$$

where $W_e = 1/T_{1e}$ is the longitudinal electron spin lattice relaxation rate and c is the concentration of radicals. The Heisenberg exchange constant k_{exch} can be estimate from EPR experiments, and in case of TEMPO in benzene and TEMPOL in water can be taken as 3.3 [30,53] and 1.9 $mM^{-1}s^{-1}$ [54], respectively.

Finally, using Eqs. (1), (7) and (8) the expression for the extrapolated to infinite power value of enhancement can be written as [52,30]:

$$E_{max}(c) = 1 - \xi\frac{r_{1,n}^{rad}c}{R_{1,n}(0) + r_{1,n}^{rad}c}\frac{1}{3}\left[3 - 4\left(2 + \frac{k_{exch}c}{W_e}\right)^{-1}\right]\frac{\gamma_e}{\gamma_n}. \tag{9}$$

Thus, the coupling factor ξ_{DNP} can be estimated both from experimentally measured as well as from the fitted concentration and power dependencies of the DNP enhancement.

3.2. NMRD

In order to test the feasibility of the application of FFC-DNP to X-nuclei, several compounds containing ^{2}H, ^{7}Li, ^{13}C in different states, solutions or confinement were studied. Depending on the particular case, the NMRD dispersion could be fitted with a suitable model.

The paramagnetic relaxation and coupling factor (see Eq. (1)) can be determined using the relaxation rates for zero-, single- and double quantum transitions, which are given as [34,49,55]:

$$w_0 = C_{dip} j(\omega_n - \omega_e, \tau_{dip}) + C_{diff} j_{diff}(\omega_n - \omega_e, \tau_{diff}) + C_{scal}[j(\omega_n - \omega_e, \tau_{scal})] \quad (10)$$

$$w_1 = \frac{3}{2} C_{dip} j(\omega_n, \tau_{dip}) + \frac{3}{2} C_{diff} j_{diff}(\omega_n, \tau_{diff}) \quad (11)$$

$$w_2 = 6 C_{dip} j(\omega_n + \omega_e, \tau_{dip}) + 6 C_{diff} j_{diff}(\omega_n + \omega_e, \tau_{diff}) \quad (12)$$

with the Lorentzian spectral density function

$$j(\omega, t) = \frac{\tau}{1 + \omega^2 \tau^2} \quad (13)$$

and the reduced spectral density function for translational diffusion [56,57]:

$$j_{diff}(z) = \frac{1 + 5z/8 + z^2/8}{1 + z + z^2/2 + z^3/6 + 4z^4/81 + z^5/81 + z^6/648} \quad (14)$$

where $z = \sqrt{\omega \tau_{diff}/2}$, and

$$\tau_{diff} = \frac{2d^2}{D_n + D_e} \quad (15)$$

with D_n and D_e being self-diffusion coefficients of the molecules containing nuclear and electron spins, respectively, and d is the minimal distance between electron and nucleus, τ_{dip}, τ_{scal} and τ_{diff} being the correlation times of dipolar, scalar interaction and interaction modulated by translational diffusion, respectively, and C_{dip}, C_{scal} and C_{diff} are corresponding prefactors. Since the Larmor nuclear frequency is negligibly small in comparison with the electron Larmor frequency, the relaxation rate of nuclear spins due to the electron-nuclear coupling in the presence of dipolar and scalar interactions is given by [58,59]:

$$\begin{aligned} R_{1para} &= R_{1dip} + R_{1scal} + R_{1diff} \\ &= C_{dip}\left[7j(\omega_e, \tau_{dip}) + 3j(\omega_n, \tau_{dip})\right] + C_{scal}[j(\omega_e, \tau_{scal})] \\ &\quad + C_{diff}\left[7j_{diff}(\omega_e, \tau_{diff}) + 3j_{diff}(\omega_n, \tau_{diff})\right] \end{aligned} \quad (16)$$

In addition, the relative contribution of scalar interaction was calculated as $M_{scal} = \lim_{\omega_{e,n} \to 0} R_{1scal}/R_{1para}$. Combining Eqs. (2) and (10)–(12) [59] one obtains for the coupling factor:

$$\xi_{NMRD} = \frac{5}{7}\left[1 - \frac{3C_{dip} j(\omega_n, \tau_{dip}) + 3C_{diff} j_{diff}(\omega_n, \tau_{diff})}{R_{1para}}\right] - \frac{12}{7} \times \frac{R_{1scal}}{R_{1para}}. \quad (17)$$

Analysis of NMRD of liquids in different porous media is presented by a variety of approaches in the literature [60–63]. Considering the absence of paramagnetic impurities in studied samples of silica particles, a mechanism of relaxation of adsorbed benzene-d_6 in silica particles caused by "reorientations mediated by translational displacements" (RMTD) was used to describe the obtained NMRD data. Thus the expression for the relaxation rate of benzene-d_6 in silica is given as:

$$R_{1RMTD} = C[j_{RMTD}(\omega) + 4j_{RMTD}(2\omega)] \quad (18)$$

where $j_{RMTD}(\omega)$, assuming the strong adsorption limit and Lévy-walk statistics with an expected Cauchy distribution, can be written as [61]

$$j_{RMTD}(\omega) = \frac{b}{4\pi \sin\left(\frac{\pi}{2}\chi\right)} c^{-(1-\chi)} \omega^{-\chi} \quad (19)$$

where b and c are constants, and χ is a parameter related with the "roughness" of the surface ($0 < \chi < 1$). The parameter c, possessing the dimension of velocity, can also be written as:

$$c = D/h \quad (20)$$

where D is the bulk diffusivity and h is the "adsorption depth", which is related with the retention time of the molecules adsorbed on the surface. Thus, the complete expression including the mentioned relaxation mechanisms is given by:

$$R_1 = R_{1,0} + R_{1,para} + R_{1,RMTD} \quad (21)$$

where $R_{1,\mathrm{RMTD}}$ equals to zero in the case of bulk liquids, when Eq. (4) is valid. Considering of relaxation rate of the system without radicals $R_{1,\mathrm{pure}} = R_{1,0} + R_{1,\mathrm{RMTD}}$ and, like in Eq. (4), the additivity of the radical induced relaxivity $r_{1\mathrm{rad}}$ [35,59] leads to:

$$R_1 = R_{1,pure} + R_{1,para} = R_{1,pure} + c r_{1rad} \quad (22)$$

A consequence of Eq. (22) is that, given two NMRD datasets corresponding to different radical concentrations c_1 and c_2, the dispersion $R_{1,\mathrm{pure}}$ of the pure substance can be recovered,

$$R_{1,pure} = \frac{c_2}{c_2 - c_1} R_{1,c_1} - \frac{c_1}{c_2 - c_1} R_{1,c_2}. \quad (23)$$

According to Eq. (23) one of the important requirements to reliably recover the NMRD of the pure substances is the precise preparation and measurement of the radical concentration in the samples. On the other hand, an even distribution of the radicals in the whole or particular parts of the system becomes mandatory. In addition, using (23) for recovering NMRD of pure samples allows to estimate relaxation times T_1 much higher than the maximum achievable for conventional FFC experiments due to hardware limitations, provided a sufficient accuracy in the measured quantities can be obtained under conditions of signal enhancement by DNP.

4. Results and discussion

4.1. Benzene-d_6

A remarkable level of OE DNP enhancement of ^{2}H NMR signal exceeding 200 at moderate power of microwave irradiation was observed in bulk deuterated benzene with 100 and 200 mM of TEMPO (Fig. 1). By comparison, the enhancement is found to be at least three times lower for benzene-d_6 in silica. This may be explained by an equivalent slowing-down of molecular motions, which modulate electron-nuclear interaction and can be related to the translational diffusion [56,57]. Despite of this reduction, the enhancement of the NMR signal is still totally sufficient to acquire ^{2}H NMRD data with high SNR.

The single line in the DNP spectra for all samples is an attribute of the so-called Heisenberg exchange effect on the hyperfine splitting of the TEMPO radical ESR spectra, when the three hyperfine lines collapse due to fast exchange processes. Moreover, Heisenberg exchange, the efficiency of which depends on the radical concentration, is more pronounced in the sample with higher concentration, thus leading to the narrower lines in the EPR and DNP spectra, respectively. In general the exchange line narrowing simplifies calculations of the coupling factor ξ due to the relevant assumption about saturation factor $s \sim 1$ at high concentrations of radicals. However, taking into account the exchange rate by fitting of the power dependencies of the DNP enhancement to Eq. (7), a more precise estimation of the coupling factor is possible. The saturation factor $s_{\max}$ obtained by fitting to Eqs. (8) and (1) and the calculated coupling factors are presented in Table 1.

The DNP enhancements $E_{\max}$, extrapolated to infinite power, are rather high in direct comparison with ^{1}H data in benzene [30]. However, $\gamma(^1\mathrm{H})/\gamma(^2\mathrm{H}) = 6.51$ and the corresponding maximal ^{2}H DNP enhancement is ~ -2140 in the dipolar interaction limit ($\xi = 0.5$) [51]. In case of the 200 mM TEMPO benzene-d_6 solution the value of $E_{\max}$ is only 25% of its theoretical maximum. One of the main reasons of low DNP enhancement of ^{2}H nuclei in comparison with ^{1}H DNP data [30], assuming the same coupling factor, is

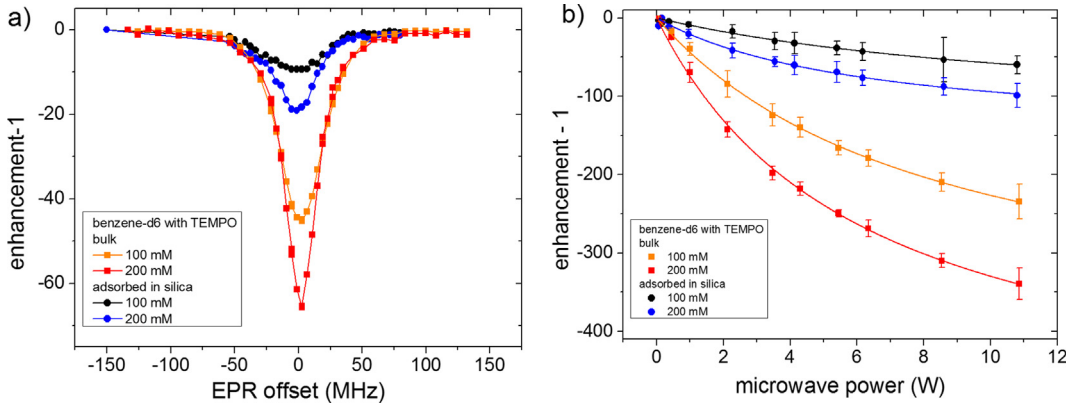

Fig. 1. ^{2}H DNP spectra at 1 W microwave power (a) and power dependencies (b) of DNP enhancement of deuterated benzene with 100 and 200 mM of TEMPO in bulk and adsorbed in silica, respectively. Lines in (b) correspond to fits by Eq. (7).

Table 1
Parameters of fitting of power dependencies of ^{2}H DNP and NMRD of benzene-d_6 with 100 and 200 mM of TEMPO in bulk and in the silica system.

TEMPO/sample	E_{max}	P_{half}	f	s_{max}	ξ_{DNP}[a]	ξ_{NMRD}[a]	t_{diff}, ps	M_{scal}
100 mM in silica	−132 ± 19	6 ± 1	0.27 ± 0.04	0.96 ± 0.02	0.12 ± 0.02	0.10 ± 0.05	60 ± 15	0.04 ± 0.01
200 mM in silica	−153 ± 12	13 ± 3	0.39 ± 0.03	0.98 ± 0.01	0.09 ± 0.01	0.11 ± 0.05	70 ± 20	0.03 ± 0.01
100 mM bulk	−419 ± 13	6.2 ± 0.4	0.35 ± 0.02	0.96 ± 0.03	0.29 ± 0.01	0.30 ± 0.04	30 ± 5	0.03 ± 0.01
200 mM bulk	−531 ± 19	8.2 ± 0.4	0.54 ± 0.02	0.98 ± 0.02	0.23 ± 0.01	0.27 ± 0.04	40 ± 6	0.05 ± 0.01

[a] The values of coupling factors are presented at 293 K and 340 Mt.

the quadrupolar relaxation, which leads to a low leakage factor, and was found to be $f = 0.54$ for the case of the 200 mM TEMPO solution. The ratio of the radical-induced relaxivities normalized to the radicals concentration $r_{1rad}(^1H)/r_{1rad}(^2H)$ for benzene [30] and deuterated benzene at polarization magnetic field (340 mT) is in the order of ~ 30, which is close to the ratio obtained in [24] and theoretical ratio of $\gamma(^1H)^2/\gamma(^2H)^2 \sim 42.5$, showing that unpaired electrons are 42.5 times more effective to increase the relaxation rate of the protons than deuterons. Additionally, the relaxation rate of the bulk deuterated benzene is ~2.5 times faster (in the non-degassed samples) [30]. Furthermore, relaxation in the system becomes faster due to the RMTD process caused by interaction of the benzene-d_6 molecules with the surface of the silica nanoparticles, which leads to the value of leakage factor of $f = 0.27$ and $f = 0.39$ for the case of 100 and 200 mM TEMPO solutions in silica, respectively. The low enhancement may as well be a result of the counteraction of dipolar and scalar relaxation mechanisms, which leads to the lower coupling factor in comparison with the system with only dipolar electron-nuclear interaction. Indeed the coupling factor obtained from DNP data for benzene-d_6 TEMPO solution is slightly reduced by ~15% in comparison with ^{1}H DNP measurements in benzene [30], which is in the range of experimental error. On the other hand, a similar effect can be caused by scalar interaction which is present on the order of a few percent (see Table 1) in the studied system. Furthermore, benzene-d_6 in silica exhibits a 2–3 times lower coupling factor reflecting a slower dynamics of both benzene-d_6 and TEMPO molecules in silica. This point is also discussed below when the T_1 dispersion results are analyzed.

The obtained DNP spectra were used to define the optimal polarization field to achieve maximum enhancement in the DNP-FFC experiments. At the same time, using high microwave power will increase the heating effect due to absorption by the sample because of dielectric losses, and by heating of the microwave resonator itself. Moreover, the dielectric constant of benzene is quite low (around 2.3) as compared with the dielectric constant of water (~80).

The DNP enhanced ^{2}H NMRD of T_1 deuterated benzene with TEMPO at different concentration and the recovered NMRD of deuterated benzene without radical using Eq. (23) in comparison with the directly measured NMRD of deuterated benzene acquired with the conventional FFC technique at thermal polarization are presented in Fig. 2.

The recovered NMRD of pure benzene-d_6 is characterized by a constant value of T_1 in the range of experimental error in the whole studied frequency range, i.e. by absence of relaxation dispersion in studied frequency range, as is expected for simple liquids [6,58]. Furthermore a good agreement between recovered and directly measured NMRD is observed according to Fig. 2(a), showing an error of around 15%.

The DNP-enhanced ^{2}H NMRD curves of benzene-d_6 in silica A380 with TEMPO are presented in Fig. 2(b). The recovered NMRD of benzene-d_6 in silica is characterized by significantly lower scattering and uncertainty in comparison with the thermal polarization data. Moreover, the scattering of the NMRD of benzene-d_6 obtained at thermal polarization is too large to even distinguish it from the results in the presence of radicals, such a distinction would necessitate a dramatic increase of the number of scans if DNP were not applied. This shows the advantage of using DNP in X-nuclei systems in order to enhance the signal for NMRD purposes.

The moderately strong dispersion of benzene-d_6 in silica is explained by the RMTD process which was reported in several basic papers [60,61,64]. The use of the spectral density function given by Eq. (19) which corresponds to the Cauchy propagator [61] results in a good fitting with corresponding parameters presented in Table 1. The parameter χ which is related with the "roughness" of the surface obtained from fitting of experimental data by (18) and (19) exhibits a value of 0.52 ± 0.02. The general theory of RMTD [39,65] assumes low adsorption limit and weak interaction for organic molecules like n-alkanes and strong interaction for polar molecules. Previous works [61,60] showed weak NMRD for non-polar organic fluids, in comparison with polar liquids such as water or DMSO with strong adsorption and values

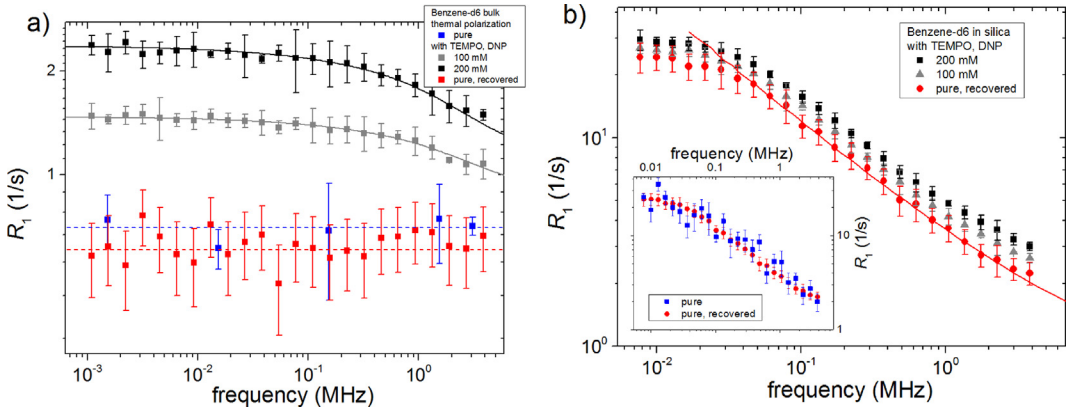

Fig. 2. ^{2}H NMRD of deuterated benzene in the bulk (a) and adsorbed in silica (b) without radicals ("pure") and with 100 and 200 mM of TEMPO in comparison with the data recovered by the difference approach. The lines represent fits by Eq. (16) (see the text) and (18) for bulk and adsorbed benzene-d_6, respectively.

of χ exceeding 0.5, which can be explained by the presence of hydroxyl groups on the surface of silica nanoparticles. In the case of benzene-d_6 in the silica system, the strong dispersion can be tentatively explained by interaction of benzene-d_6 molecules and hydroxyl groups via π-electron interaction [66,67] which renders the molecules preferentially oriented at the surface.

4.2. ^{7}Li in aqueous solution

^{7}Li with ~93% natural abundance and a spin 3/2 is an isotope occasionally used in DNP studies [21,51,68]. Materials containing lithium are used in a wide range of applications including batteries, semiconductors, lasers etc.

S-band ^{7}Li DNP spectra of 6 M LiCl aqueous solution with TEMPOL radical presented in Fig. 3 exhibit positive OE with the shape of the spectra corresponding to the ESR lineshape due to hyperfine splitting by the ^{14}N (I = 1) nucleus in the TEMPOL radical. Contrary to TEMPO in the benzene-d_6 solution with a concentration of 100 mM, the three hyperfine lines are still observable in the aqueous LiCl solution with 89 mM TEMPOL, which is a consequence of a slower Heisenberg exchange in comparison with the benzene-d_6 solution. On the other hand, according to the literature [53,69] three lines collapse to one line in pure aqueous TEMPOL solution at concentration higher than 50–70 mM – this reflects the strong LiCl influence on the dynamics of the TEMPOL radical. The analysis of the linewidth dependence of the EPR line of TEMPOL in LiCl aqueous solution (data not shown) exhibits slower Heisenberg exchange with an exchange constant of 0.9 ± 0.1 mM^{-1}s^{-1} in comparison with pure water TEMPOL solution (k_{exch} = 1.9 mM^{-1}-s^{-1}) [69].

The obtained coupling factor from DNP experiments using (9) is relatively low with ~0.06 at 3.5 mM of TEMPOL, restricting the maximum enhancement to less than 60, which is about 3% of the maximal theoretical enhancement value of $\gamma(e)/\gamma(^{7}Li) \sim 1693$. The value of T_{1e} was taken from [53] as 287 ± 30 ns to calculate the coupling factor at 3.5 mM TEMPOL in LiCl aqueous solution. An increase of the TEMPOL concentration does not lead to the expected increasing of the enhancement [30,52], one rather observes the opposite effect of a decrease of E_{max}. The T_{1e} concentration dependence was calculated using both, Eq. (9) and the experimentally obtained E_{max}(c). Both are represented in Fig. 4. Therefore the coupling parameter was fixed at the value of 0.057 ± 0.004 for the dataset of samples with TEMPOL concentrations above 3.5 mM, when only the parameter $W_e = 1/2T_{1e}$ was fitted. To the knowledge of the authors, there is no information in the literature about concentration dependence of the coupling factor. Even though, one cannot exclude that the scalar contribution might be concentration dependent, leading to the changing of the coupling factor. On the other hand it should be reflected on the relaxation dispersion as well, which was not observed in the results. The obtained concentration dependence of T_{1e} exhibits a pronounced decrease of the relaxation time down to 1 ns with increasing of concentration to 85 mM of TEMPOL. Actually, a relatively strong concentration dependence of the electron longitudinal relaxation time T_{1e} was indeed reported [53,70] in solutions of different nitroxide radicals in the low concentration range,

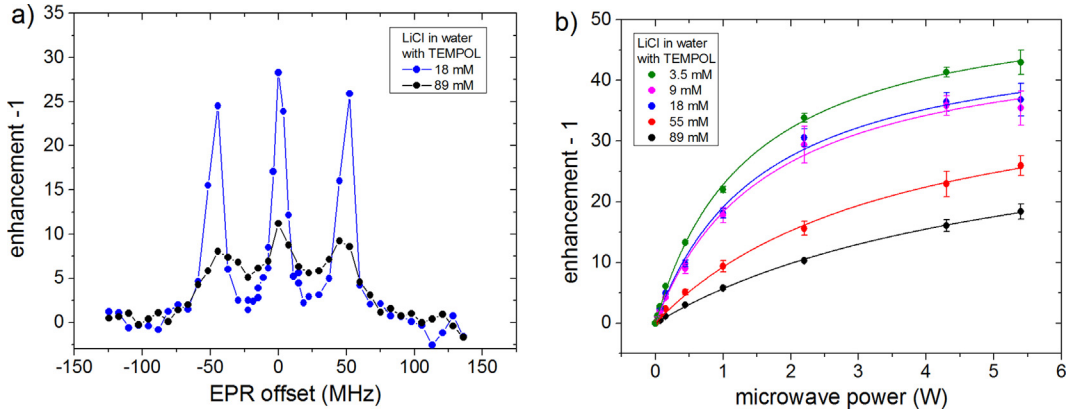

Fig. 3. ^{7}Li DNP spectra (a) of 6 M LiCl in H_2O at 2.2 W with 18 mM and 89 mM TEMPOL and power dependencies of DNP enhancement (b) at different concentrations of TEMPOL. Lines in (b) correspond to fits by Eq. (7).

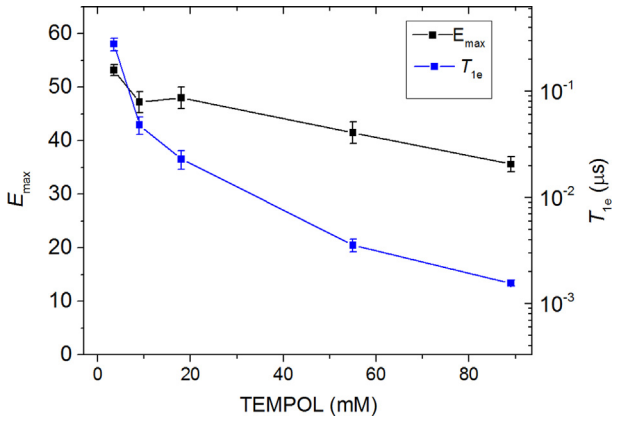

Fig. 4. Concentration dependences of ^{7}Li extrapolated enhancement E_{max} obtained with Eq. (7) and electron relaxation time T_{1e} obtained using Eq. (9).

approaching a constant value of around ~100 ns above 10 mM of radical concentration. On the other hand the presence of Li+ ions in aqueous solution may affect the dynamics of TEMPOL radicals leading to slower Heisenberg exchange and lower values of the T_{1e} electron relaxation time. However, the thorough analysis of obtained concentration dependence of T_{1e} is beyond the goal of this work.

The measured ^{7}Li NMRD of LiCl in aqueous solution (Fig. 5) exhibits strong dispersion at Larmor frequencies above 100 kHz with a well-pronounced low frequency plateau, both features following from electron-nuclear interaction modulated by the relative dynamics of radical and lithium ions. The different dynamics of nitroxide radicals was reported in aqueous solutions [1,53] in comparison with organic non-polar organic solvents such as benzene [30], n-alkanes [71] etc, exhibiting an increasing rotational diffusion contribution due to a competition of nitroxide radical and water molecules for the hydration of salt ions [21].

The observation of a net positive OE DNP enhancement reflects the fact that a significant, and dominating, contribution of scalar interaction between the nuclear spin of lithium ions and the electron spins of TEMPOL radical exists. A prevailing scalar contribution of up to 70% was reported [21] for a low field ^{7}Li DNP study in aqueous solution with different radicals. The relative contribution of scalar interaction was found in the range of 58–68 % (see

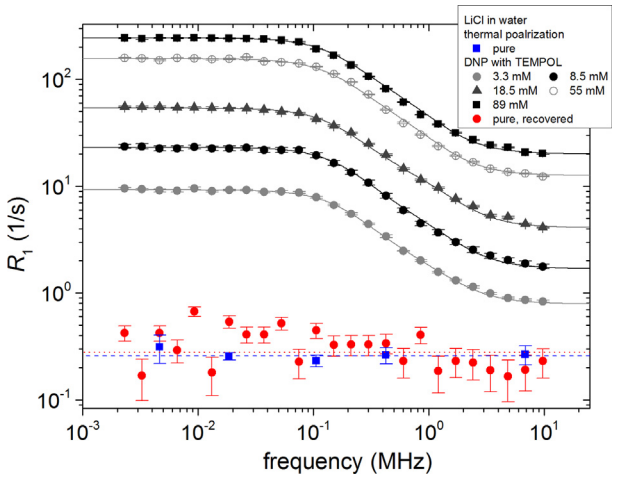

Fig. 5. ^{7}Li NMRD of 6 M aqueous solution of LiCl with TEMPOL at different concentration. The recovered NMRD of the solution is presented for comparison with directly measured T_1 values of the pure 6 M LiCl aqueous solution. The solid lines present fitting of experimental data by Eq. (16).

Table 2) using fitting of experimental data with Eq. (16) considering a Lorentzian spectral density (13) and a non-zero contribution of the scalar term in (16). The results of the fitting procedure are presented in Table 2.

The coupling factor values obtained from NMRD data (see Table 2) possess somewhat higher uncertainties, however being in good agreement with value of coupling factor obtained from DNP data.

The value of the relaxation time of pure LiCl aqueous solution without TEMPOL measured at several values of the magnetic field strength lacks a significant dispersion with $T_1 = (3.7 \pm 0.3)$ s, which is common for low viscous liquids and solutions [6] at ambient temperature in the studied frequency range. Furthermore, the recovered NMRD of pure LiCl aqueous solution using the difference approach (23) also shows no dispersion and a $T_1 = (3.4 \pm 0.5)$ s in good agreement with values obtained by conventional FFC at thermal polarization in pure LiCl solutions.

4.3. ^{13}C-enriched benzene-d_6

Benzene-d_6 enriched at 99% with ^{13}C was used to calibrate the hardware and adjust the polarization field to achieve maximum enhancement (see Fig. 6). In addition, using a degassed sample allows to estimate the effect of oxygen on the achieved DNP enhancement. One broad line in the DNP spectrum is observed instead of the three hyperfine lines of TEMPO similar to the situation found with deuterated benzene, the Heisenberg exchange process (with $k = 3.3$ mM^{-1}s^{-1} [30]) being efficient already at 70 mM concentration of TEMPO. The corresponding power dependence of ^{13}C DNP enhancement was obtained and fitted with Eq. (7), showing the values of E_{max} of -294 ± 4 and -344 ± 11 for 135 mM and 320 mM TEMPO concentration, respectively, and $E_{max} = 257 \pm 4$ for 70 mM of TEMPO in degassed benzene-d_6. The estimated level of DNP enhancement in non-enriched benzene-d_6 samples (see Table 3) is in good agreement with the results for enriched benzene-d_6, considering ~1.1% of natural abundance of ^{13}C isotope and using the thermal polarization signal of the ^{13}C enriched benzene-d_6 with TEMPO as a reference.

The deviating saturation behavior for the degassed sample reflects the effect of oxygen on the electron relaxation time leading to a 30% higher enhancement values at maximum power for the degassed sample. However, the corresponding value of maximal enhancement E_{max} is still higher for the solution with higher concentration of TEMPO, in good agreement with literature [30,52,69]. Thus, the optimal effective enhancement at moderate power can be reached even at moderate concentrations with degassing, considering a possible concentration dependence of the T_{1e} electron relaxation time in degassed liquids [53] and its effect on the calculated parameters, e.g. using Eq. (9). The optimal values of power of microwave field of around 2 W and 3.5 W were found for 70 mM and 350 mM TEMPO concentration, which was used to obtain NMRD curves enhanced by DNP, presented in Fig. 7.

A simple calculation using the DNP experimental data of ^{13}C enriched benzene-d_6 allows estimation of the expected level of DNP enhanced NMR signal with natural abundance of ^{13}C nuclei in benzene-d_6 (see Table 3). The corresponding NMRD of enriched benzene-d_6 with 70 mM, 135 mM and 320 mM were measured to obtain values of the relaxation time T_1 in pure ^{13}C enriched benzene-d_6 (combination of 135 mM and 320 mM of TEMPO in benzene-d_6), resulting in a value of $T_1 \approx 12$ s. The reliable comparison with independently measured T_1 in pure benzene-d_6 is cumbersome due to the low thermal polarization of ^{13}C nuclei and the restriction of the hardware which limits measurements of relaxation times $T_1 > 10$ s. However, the obtained value of relaxation time in ^{13}C enriched benzene-d_6 is in good agreement with literature data [72], taking into account that the relaxation time

Table 2
Experimental and fitting parameters of power dependencies of DNP enhancement of ^{7}Li of 6 M LiCl in water solution with different TEMPOL concentrations.

TEMPOL mM	E_{max}	P_{half}	f	s_{max}	ξ_{DNP}[a]	ξ_{NMRD}[a]	t_{dip}, ps	t_{scal}, ps	M_{scal}
3.5	53 ± 1	1.4 ± 0.1	0.86 ± 0.01	0.65 ± 0.02	−0.057 ± 0.004	−0.05 ± 0.02	40 ± 5	450 ± 75	0.60 ± 0.05
9	47 ± 2	1.6 ± 0.2	0.94 ± 0.01	0.52 ± 0.01	−0.057[b]	−0.06 ± 0.02	35 ± 6	420 ± 50	0.65 ± 0.04
18	48 ± 2	1.6 ± 0.2	0.97 ± 0.01	0.52 ± 0.01	−0.057[b]	−0.06 ± 0.02	39 ± 4	440 ± 40	0.63 ± 0.02
55	42 ± 2	3.6 ± 0.3	0.99 ± 0.01	0.43 ± 0.02	−0.057[b]	−0.04 ± 0.01	42 ± 3	480 ± 35	0.58 ± 0.02
89	39 ± 2	5.5 ± 0.4	0.99 ± 0.01	0.40 ± 0.02	−0.057[b]	−0.05 ± 0.01	49 ± 4	495 ± 25	0.68 ± 0.04

[a] The values of coupling factors are presented at 293 K and 70 mT.
[b] The value of coupling factor was fixed for concentrations of TEMPOL above 3.5 mM.

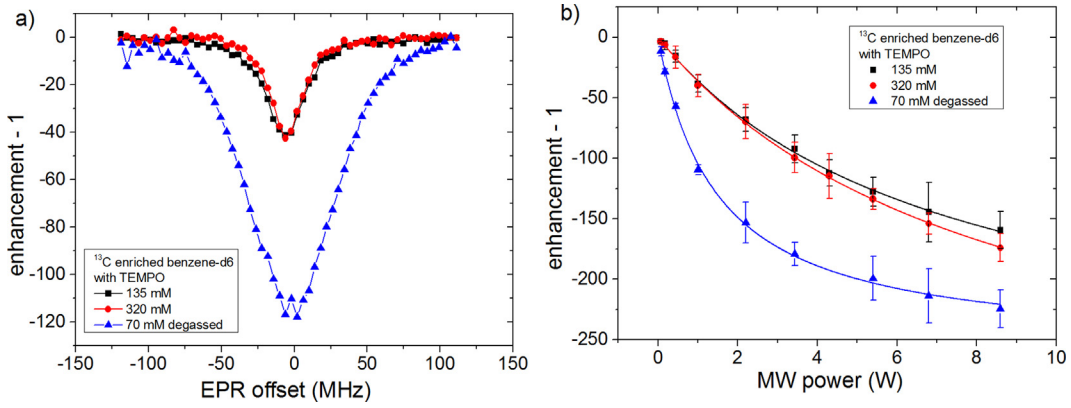

Fig. 6. ^{13}C DNP spectrum (a) at 1 W and power dependency (b) of ^{13}C *enriched* benzene-d_6 with TEMPO. Lines in (b) correspond to fits by Eq. (7).

Table 3
Parameters of fitting of power dependencies of ^{13}C DNP and NMRD of ^{13}C enriched benzene-d_6 with 70 and 350 mM of TEMPO.

Sample	TEMPO	E_{max}	P_{half}	f	s_{max}	ξ_{DNP}[a]	ξ_{NMRD}[a]	t_{scal}, ps	t_{diff}, ps	M_{scal}
$^{13}C_6D_6$	135 mM	−294 ± 4	7.2 ± 0.1	0.93 ± 0.02	0.96 ± 0.01	0.13 ± 0.01	0.13 ± 0.02	21 ± 4	62 ± 10	0.10 ± 0.02
	320 mM	−344 ± 11	8.5 ± 0.4	0.96 ± 0.02	0.97 ± 0.01	0.14 ± 0.01	0.15 ± 0.02	15 ± 5	55 ± 11	0.09 ± 0.02
	70 mM[b]	−257 ± 4	1.5 ± 0.1	0.85 ± 0.03	0.94 ± 0.01	0.13 ± 0.01	0.15 ± 0.2	21 ± 4	60 ± 10	0.10 ± 0.02
C_6D_6	85 mM	−248 ± 65	6.5 ± 3.8	0.89 ± 0.06	0.97 ± 0.01	0.13 ± 0.05	0.13 ± 0.06	18 ± 8	65 ± 28	0.10[c]
	155 mM	−310 ± 80	10.1 ± 4.8	0.94 ± 0.06	0.99 ± 0.01	0.12 ± 0.06	0.14 ± 0.05	23 ± 11	58 ± 21	0.10[c]

[a] The values of coupling factors are presented at 293 K and 340 mT.
[b] Degassed.
[c] The value of scalar contribution M_{scal} was fixed as 0.1 for better fit.

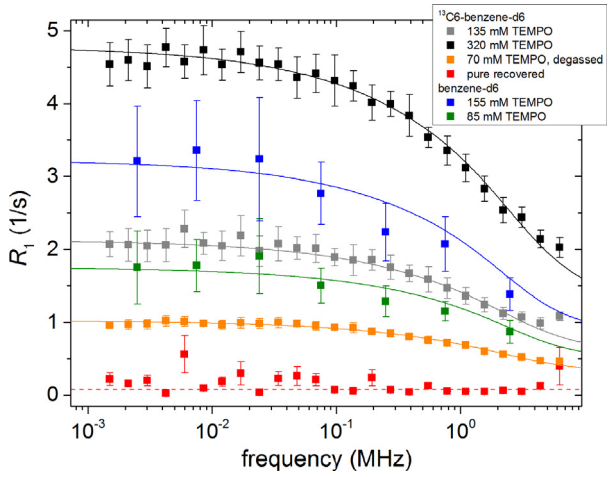

Fig. 7. ^{13}C NMRD of enriched deuterated benzene-d_6 with TEMPO in comparison with recovered NMRD of the pure substance and with NMRD of benzene-d_6 with natural abundance of ^{13}C. The solid lines present fitting of experimental data by Eq. (16).

of ^{13}C in enriched benzene-d_6 is about half that of benzene-d_6 with natural abundance of ^{13}C isotope ($T_1 \approx 20$ s at ambient temperature in non-degassed sample [72]) due to the additional contribution from ^{13}C–^{13}C dipolar interaction, which can be roughly estimated based on the ratio $\gamma(^{13}C)^2/\gamma(^{2}H)^2 \approx 2.5$ and C–C and C–D interatomic distances in d_6-benzene (~0.14 nm and 0.11 nm, respectively), using expression for spin–lattice relaxation rate [50,55,58]. However, the NMRD data quality for the samples of benzene-d_6 with natural abundance of ^{13}C with 85 mM and 155 mM of TEMPO was not sufficient to recover long T_1 values. This is due to the fact that the recovered NMRD values from Eq. (23) are characterized by a low relaxation rate in comparison with NMRD of the samples with radicals. In this case, a moderate scattering or error of the $R_{1,c1}$ and $R_{1,c2}$ data leads to the unreliably recovered R_1 of the pure substance. One possible solution is the increase of SNR by increasing DNP enhancement and/or sensitivity improvement of the hardware. On the other hand, the temporal and spatial magnetic field instability characteristic of the FFC method may increase the uncertainty in the experimental data affecting the recovery of the NMRD by using the suggested method. Nevertheless, this shows the high potential of the difference approach for

studying X-nuclei systems when direct measurement of the relaxation time is limited.

The application of Eq. (16) for fitting of the NMRD data confirms literature results of correlation times and the contribution of scalar interaction as well. The coupling factor values obtained by both DNP and NMRD dataset shows good agreement with literature data [1]. However the coupling factor value of ~0.13 (at 293 K and 0.34 T) is 2–3 times less than the reported value for benzene ^{1}H DNP [5,30]. This can be explained by a significant contribution of scalar interaction to ^{13}C relaxation on the order of 10% as obtained from fitting the NMRD data by (16), where it was assumed that the electron-nuclear interaction is modulated by translational diffusion and additional scalar interaction with a corresponding spectral density function which is given by (13) and (14).

5. Conclusion and perspectives

Molecular dynamics investigations of X-nuclei systems by means of DNP FFC were demonstrated. DNP enhancement up to ~300 of ^{2}H nuclei of deuterated benzene at ambient temperature and X-band was achieved and was employed for increasing the sensitivity of ^{2}H NMRD measurements, showing an appreciable increase of SNR, corresponding to DNP enhancement. The perceptible positive ^{7}Li DNP enhancement by OE up to ~40 shows prevailing scalar contribution in LiCl water solution.

In the case of the ^{13}C DNP FFC study, a level of enhancement up to ~250 was reached, allowing for the first time to obtain ^{13}C NMR signal to perform NMRD at natural abundance of ^{13}C in benzene-d_6 at ambient temperature. This result is extremely important because of its outstanding potential to measure NMRD of organic compounds without the need of isotope enrichment. Of particular interest is the study of ^{13}C relaxation dispersion in the context of the development of new contrast agents for ^{13}C MRI applications where the dependence of the relaxivity on the magnetic field strength allows optimizing experimental condition for a higher efficiency of contrast agents. The use of more recent polarizing agents in hyperpolarization techniques such as NV-centers, parahydrogen etc. requires additional information about the relaxation dispersion of nuclei at low magnetic field, which represents the conditions of transport in between the location of hyperpolarization and the actual MRI scanner or high-field spectrometer.

X nuclei DNP-FFC relaxometry opens up a new pathway to specific molecular dynamics investigations that have previously suffered from low signal-to-noise ratio or were entirely impossible due to low sample amounts. The simplification of dynamics studies by studying ^{2}H relaxation which contains only intramolecular contributions, and the observation of monatomic ionic mobility and interaction which was shown for, but is not limited to, ^{7}Li nuclei are but two examples for this approach. The difference method used for recovering relaxation dispersion of pure species by eliminating the additional relaxivity of the radicals was proven to work also for nuclei other than ^{1}H. The recovered dispersion functions were shown to be in good agreement with thermal data of the pure substances where these were within reach of the instrument's sensitivity. Dispersion of the longitudinal relaxation times not only provides a basis for developing models for molecular dynamics, but also deliver an independent means of determining molecule-radical interaction or quantification of coupling factors and distinction of competing relaxation mechanisms, which complement the parameters extracted from lineshape analyses and power-dependence measurements of the enhancement factor. Given sufficient solubility of suitable stable radical species, the difference method can be applied to a wider range of X nuclei in solutions and possibly solids, the main limitations being given by the minimum nuclear and electron relaxation times of the systems.

Acknowledgments

This work was supported by the Deutsche Forschungsgemeinschaft DFG (Grant STA 511/15-1).

References

[1] O. Neudert, C. Mattea, S. Stapf, M. Reh, H.W. Spiess, K. Münnemann, Fast-field-cycling relaxometry enhanced by dynamic nuclear polarization, Microporous Mesoporous Mater. 205 (2015) 70–74.
[2] O. Neudert, M. Reh, H.W. Spiess, K. Munnemann, X-Band DNP hyperpolarization of viscous liquids and polymer melts, Macromol. Rapid. Commun. 36 (2015) 885–889.
[3] B. Gizatullin, M. Gafurov, A. Rodionov, G. Mamin, C. Mattea, S. Stapf, S. Orlinskii, Proton-radical interaction in crude Oil—A combined NMR and EPR study, Energy Fuels 32 (2018) 11261–11268.
[4] O. Neudert, C. Mattea, S. Stapf, Molecular dynamics-based selectivity for fast-field-cycling relaxometry by overhauser and solid effect dynamic nuclear polarization, J. Magn. Reson. 276 (2017) 113–121.
[5] B. Gizatullin, I. Shikhov, C. Arns, C. Mattea, S. Stapf, On the influence of wetting behaviour on relaxation of adsorbed liquids - A combined NMR,EPR and DNP study of aged rocks, Magn. Reson. Imaging 56 (2019) 96–102.
[6] R. Kimmich, E. Anoardo, Field-cycling NMR relaxometry, Prog. Nucl. Magn. Reson. Spectrosc. 44 (2004) 257–320.
[7] G. Parigi, N. Rezaei-Ghaleh, A. Giachetti, S. Becker, C. Fernandez, M. Blackledge, C. Griesinger, M. Zweckstetter, C. Luchinat, Long-range correlated dynamics in intrinsically disordered proteins, J. Am. Chem. Soc. 136 (2014) 16201–16209.
[8] J. Struppe, F. Noack, Angular and frequency dependent spin relaxation study of liquid crystalline cyanobiphenyls, Liq. Cryst. 20 (2007) 595–606.
[9] E. Anoardo, F. Bonetto, R. Kimmich, Apparent low-field spin-lattice dispersion in the smectic-A mesophase of thermotropic cyanobiphenyls, Phys. Rev. E Stat. Nonlin. Soft. Matter. Phys. 68 (2003) 022701.
[10] J.-P. Korb, N. Vorapalawut, B. Nicot, R.G. Bryant, Relation and correlation between NMR relaxation times, diffusion coefficients, and viscosity of heavy crude oils, J. Phys. Chem. C 119 (2015) 24439–24446.
[11] S. Stapf, A. Ordikhani-Seyedlar, N. Ryan, C. Mattea, R. Kausik, D.E. Freed, Y.-Q. Song, M.D. Hürlimann, Probing maltene-asphaltene interaction in crude oil by means of NMR relaxation, Energy Fuels 28 (2014) 2395–2401.
[12] R. Kimmich, N. Fatkullin, Self-diffusion studies by intra- and inter-molecular spin-lattice relaxometry using field-cycling: Liquids, plastic crystals, porous media, and polymer segments, Prog. Nucl. Magn. Reson. Spectrosc. 101 (2017) 18–50.
[13] D. Kruk, O. Lips, Field-dependent nuclear relaxation of spins 1/2 induced by dipole-dipole couplings to quadrupole spins: LaF3 crystals as an example, J. Magn. Reson. 179 (2006) 250–262.
[14] F. Fujara, D. Kruk, A.F. Privalov, Solid state field-cycling NMR relaxometry: instrumental improvements and new applications, Prog. Nucl. Magn. Reson. Spectrosc. 82 (2014) 39–69.
[15] G. Liu, M. Levien, N. Karschin, G. Parigi, C. Luchinat, M. Bennati, One-thousand-fold enhancement of high field liquid nuclear magnetic resonance signals at room temperature, Nat. Chem. 9 (2017) 676–680.
[16] J.H. Ardenkjaer-Larsen, B. Fridlund, A. Gram, G. Hansson, L. Hansson, M.H. Lerche, R. Servin, M. Thaning, K. Golman, Increase in signal-to-noise ratio of >10,000 times in liquid-state NMR, Proc. Natl. Acad. Sci. U. S. A. 100 (2003) 10158–10163.
[17] G. Jeschke, A new mechanism for chemically induced dynamic nuclear polarization in the solid state, J. Am. Chem. Soc. 120 (1998) 4425–4429.
[18] I.J. Day, R. Wain, K. Tozawa, L.J. Smith, P.J. Hore, Photo-CIDNP NMR spectroscopy of a heme-containing protein, J. Magn. Reson. 175 (2005) 330–335.
[19] R.A. Green, R.W. Adams, S.B. Duckett, R.E. Mewis, D.C. Williamson, G.G. Green, The theory and practice of hyperpolarization in magnetic resonance using parahydrogen, Prog. Nucl. Magn. Reson. Spectrosc. 67 (2012) 1–48.
[20] D.A. Barskiy, S. Knecht, A.V. Yurkovskaya, K.L. Ivanov, SABRE: Chemical kinetics and spin dynamics of the formation of hyperpolarization, Prog. Nucl. Magn. Reson. Spectrosc. 114–115 (2019) 33–70.
[21] J.A. Potenza, J.W. Linowski, Dynamic polarization of ^{7}Li nuclei in solution, J. Chem. Phys. 54 (1971) 4095–4099.
[22] V.A. Atsarkin, A.V. Kessenikh, Dynamic nuclear polarization in solids: the birth and development of the many-particle concept, Appl. Magn. Reson. 43 (2012) 7–19.
[23] A.E. Dementyev, D.G. Cory, C. Ramanathan, Dynamic nuclear polarization in silicon microparticles, Phys. Rev. Lett. 100 (2008) 127601.
[24] R.D. Bates, E.H. Poindexter, B.E. Wagner, Dynamic nuclear polarization studies of intermolecular coupling of deuteron and unpaired electron spins, J. Chem. Phys. 59 (1973) 3031–3037.
[25] O. Neudert, H.P. Raich, C. Mattea, S. Stapf, K. Münnemann, An alderman-grant resonator for S-band dynamic nuclear polarization, J. Magn. Reson. 242 (2014) 79–85.
[26] O. Neudert, C. Mattea, S. Stapf, A compact X-band resonator for DNP-enhanced fast-field-cycling NMR, J. Magn. Reson. 271 (2016) 7–14.
[27] O. Neudert, D.G. Zverev, C. Bauer, P. Blümler, H.W. Spiess, D. Hinderberger, K. Münnemann, Overhauser DNP and EPR in a mobile setup: influence of magnetic field inhomogeneity, Appl. Magn. Reson. 43 (2012) 149–165.

[28] C. Griesinger, M. Bennati, H.M. Vieth, C. Luchinat, G. Parigi, P. Hofer, F. Engelke, S.J. Glaser, V. Denysenkov, T.F. Prisner, Dynamic nuclear polarization at high magnetic fields in liquids, Prog. Nucl. Magn. Reson. Spectrosc. 64 (2012) 4–28.
[29] B. Gizatullin, O. Neudert, S. Stapf, C. Mattea, Dynamic nuclear polarization fast field cycling method for the selective study of molecular dynamics in block copolymers, ChemPhysChem 18 (2017) 2347–2356.
[30] O. Neudert, C. Mattea, H.W. Spiess, S. Stapf, K. Münnemann, A comparative study of ^{1}H and ^{19}F Overhauser DNP in fluorinated benzenes, Phys. Chem. Chem. Phys. 15 (2013) 20717–20726.
[31] P. Niedbalski, C. Parish, Q. Wang, A. Kiswandhi, L. Lumata, 13C Dynamic nuclear polarization using derivatives of TEMPO free radical, Appl. Magn. Reson. 48 (2017) 933–942.
[32] J. Hu, N. Whiting, P. Bhattacharya, Hyperpolarization of Silicon Nanoparticles with TEMPO Radicals, J. Phys. Chem. C 122 (2018) 10575–10581.
[33] L. Lumata, S.J. Ratnakar, A. Jindal, M. Merritt, A. Comment, C. Malloy, A.D. Sherry, Z. Kovacs, BDPA: an efficient polarizing agent for fast dissolution dynamic nuclear polarization NMR spectroscopy, Chemistry 17 (2011) 10825–10827.
[34] N. Bloembergen, Proton relaxation times in paramagnetic solutions, J. Chem. Phys. 27 (1957) 572–573.
[35] N. Bloembergen, L.O. Morgan, Proton relaxation times in paramagnetic solutions, effects of electron spin relaxation, J. Chem. Phys. 34 (1961) 842–850.
[36] B. Gizatullin, C. Mattea, S. Stapf, Hyperpolarization by DNP and Molecular Dynamics: Eliminating the Radical Contribution in NMR Relaxation (submitted for publication).
[37] M. Kehr, N. Fatkullin, R. Kimmich, Deuteron and proton spin-lattice relaxation dispersion of polymer melts: intrasegment, intrachain, and interchain contributions, J. Chem. Phys. 127 (2007) 084911.
[38] G. Schauer, R. Kimmich, W. Nusser, Deuteron field-cycling relaxation spectroscopy and translational water diffusion in protein hydration shells, Biophys. J. 53 (1988) 397–404.
[39] S. Stapf, R. Kimmich, R. Seitter, Proton and deuteron field-cycling NMR relaxometry of liquids in porous glasses: Evidence for Levy-walk statistics, Phys. Rev. Lett. 75 (1995) 2855–2858.
[40] A. Lozovoi, C. Mattea, N. Fatkullin, S. Stapf, Segmental dynamics of entangled poly(ethylene oxide) melts: deviations from the tube-reptation model, Macromolecules 51 (2018) 10055–10064.
[41] R. Meier, D. Kruk, A. Bourdick, E. Schneider, E.A. Rössler, Inter- and intramolecular relaxation in molecular liquids by field cycling ^{1}H NMR relaxometry, Appl. Magn. Reson. 44 (2012) 153–168.
[42] J. Gabriel, O.V. Petrov, Y. Kim, S.W. Martin, M. Vogel, Lithium ion dynamics in Li_2S+GeS_2+GeO_2 glasses studied using (7)Li NMR field-cycling relaxometry and line-shape analysis, Solid State Nucl. Magn. Reson. 70 (2015) 53–62.
[43] T. Orlando, R. Dervisoglu, M. Levien, I. Tkach, T.F. Prisner, L. Andreas, V.P. Denysenkov, M. Bennati, Dynamic nuclear polarization of (1)(3)C nuclei in the liquid state over a 10 Tesla field range, Angew. Chem. Int. Ed. Engl. 58 (2018) 1402–1406.
[44] M. Brodrecht, K. Herr, S. Bothe, M. de Oliveira Jr., T. Gutmann, G. Buntkowsky, Efficient building-blocks for solid state peptide synthesis of spin-labeled peptides for EPR and DNP applications, Chemphyschem 20 (2019) 1475–1487.
[45] S.J. Nelson, J. Kurhanewicz, D.B. Vigneron, P.E. Larson, A.L. Harzstark, M. Ferrone, M. van Criekinge, J.W. Chang, R. Bok, I. Park, G. Reed, L. Carvajal, E.J. Small, P. Munster, V.K. Weinberg, J.H. Ardenkjaer-Larsen, A.P. Chen, R.E. Hurd, L.I. Odegardstuen, F.J. Robb, J. Tropp, J.A. Murray, Metabolic imaging of patients with prostate cancer using hyperpolarized [1-(1)(3)C]pyruvate, Sci. Transl. Med. 5 (2013) 198ra108.
[46] X. Wang, W.C. Isley Iii, S.I. Salido, Z. Sun, L. Song, K.H. Tsai, C.J. Cramer, H.C. Dorn, Optimization and prediction of the electron-nuclear dipolar and scalar interaction in (1)H and (13)C liquid state dynamic nuclear polarization, Chem. Sci. 6 (2015) 6482–6495.
[47] O. Neudert, C. Mattea, S. Stapf, Application of CPMG acquisition in Fast-Field-Cycling relaxometry, Microporous Mesoporous Mater. 269 (2018) 103–108.
[48] K.H. Hausser, D. Stehlik, Dynamics nuclear polarization in liquid, Adv. Magn. Reson. (1968) 79–139.
[49] E. Ravera, C. Luchinat, G. Parigi, Basic facts and perspectives of Overhauser DNP NMR, J. Magn. Reson. 264 (2016) 78–87.
[50] A. Abragam, The Principles of Nuclear Magnetism, Oxford University Press, Oxford, 1961.
[51] W. Müller-Warmuth, K. Meise-Gresch, Molecular motions and interactions as studied by dynamic nuclear polarization (DNP) in free radical, Solutions 11 (1983) 1–45.
[52] B.D. Armstrong, S. Han, A new model for Overhauser enhanced nuclear magnetic resonance using nitroxide radicals, J. Chem. Phys. 127 (2007) 104508.
[53] J.R. Biller, J.E. McPeak, S.S. Eaton, G.R. Eaton, Measurement of T1e, T1N, T1HE, T2e, and T2HE by Pulse EPR at X-band for nitroxides at concentrations relevant to solution DNP, Appl. Magn. Reson. 49 (2018) 1235–1251.
[54] Y. Sueishi, N. Nishimura, K. Hirata, K. Kuwata, ESR studies of solvent and pressure effects on spin exchange of nitroxide radicals in solution, Bull. Chem. Soc. Jpn. 61 (1988) 4253–4257.
[55] I. Solomon, Relaxation processes in a system of two spins, Phys. Rev. 99 (1955) 559–565.
[56] L.-P. Hwang, J.H. Freed, Dynamic effects of pair correlation functions on spin relaxation by translational diffusion in liquids, J. Chem. Phys. 63 (1975) 4017.
[57] J.H. Freed, Dynamic effects of pair correlation functions on spin relaxation by translational diffusion in liquids. II. Finite jumps and independent T1 processes, J. Chem. Phys. 68 (1978) 4034–4037.
[58] R. Kimmich, NMR: Tomography, Diffusometry, Relaxometry, Springer, Berlin, New York, 1997.
[59] M. Bennati, C. Luchinat, G. Parigi, M.-T. Turke, Water ^{1}H relaxation dispersion analysis on a nitroxide radical provides information on the maximal signal enhancement in Overhauser dynamic nuclear polarization experiments, Phys. Chem. Chem. Phys. 12 (2010) 5902.
[60] S. Stapf, R. Kimmich, J. Niess, Microstructure of porous media and field-cycling nuclear magnetic relaxation spectroscopy, J. Appl. Phys. 75 (1994) 529–537.
[61] T. Zavada, R. Kimmich, The anomalous adsorbate dynamics at surfaces in porous media studied by nuclear magnetic resonance methods. The orientational structure factor and Lévy walks, J. Chem. Phys. 109 (1998) 6929–6939.
[62] S. Godefroy, J.P. Korb, M. Fleury, R.G. Bryant, Surface nuclear magnetic relaxation and dynamics of water and oil in macroporous media, Phys. Rev. E Stat. Nonlin. Soft. Matter. Phys. 64 (2001) 021605.
[63] J.P. Korb, Multiscale nuclear magnetic relaxation dispersion of complex liquids in bulk and confinement, Prog. Nucl. Magn. Reson. Spectrosc. 104 (2018) 12–55.
[64] R. Kimmich, S. Stapf, P. Callaghan, A. Coy, Microstructure of porous media probed by NMR techniques in sub-micrometer length scales, Magn. Reson. Imaging 12 (1994) 339–343.
[65] O.V. Bychuk, B. O'Shaughnessy, Anomalous surface diffusion: A numerical study, J. Chem. Phys. 101 (1994) 772.
[66] H. Zhao, S. Tang, Q. Zhang, L. Du, Weak hydrogen bonding competition between O-H···π and O–H···Cl, RSC Adv. 7 (2017) 22485–22491.
[67] K.P. Gierszal, J.G. Davis, M.D. Hands, D.S. Wilcox, L.V. Slipchenko, D. Ben-Amotz, π-Hydrogen bonding in liquid water, J. Phys. Chem. Lett. 2 (2011) 2930–2933.
[68] T. Chakrabarty, N. Goldin, A. Feintuch, L. Houben, M. Leskes, Paramagnetic metal-ion dopants as polarization agents for dynamic nuclear polarization NMR spectroscopy in inorganic solids, ChemPhysChem 19 (2018) 2139–2142.
[69] M.T. Turke, M. Bennati, Saturation factor of nitroxide radicals in liquid DNP by pulsed ELDOR experiments, Phys. Chem. Chem. Phys. 13 (2011) 3630–3633.
[70] J.L. Yoder, P.E. Magnelind, M.A. Espy, M.T. Janicke, Exploring the limits of overhauser dynamic nuclear polarization (O-DNP) for portable magnetic resonance detection of low γ nuclei, Appl. Magn. Reson. 49 (2018) 707–724.
[71] R.L. Donkers, D.G. Leaist, Diffusion of free radicals in solution.TEMPO, diphenylpicrylhydrazyl, and nitrosodisulfonate, J. Phys. Chem. B 101 (1997) 304–308.
[72] G.C. Levy, J.D. Cargioli, F.A.L. Anet, Carbon-13 spin-lattice relaxation in benzene and substituted aromatic compounds, J. Am. Chem. Soc. 95 (1973) 1527–1535.